Effects of a Heavy Atom on Molecular Order and Morphology in Conjugated Polymer:Fullerene Photovoltaic Blend Thin Films and Devices

Wing C. Tsoi,[†,‡] David T. James,[†] Ester Buchaca Domingo,[§] Jong Soo Kim,[†] Mohammed Al-Hashimi,[⊥] Craig E. Murphy,[‡] Natalie Stingelin,[§] Martin Heeney,[⊥] and Ji-Seon Kim[†,#,*]

[†]Department of Physics & Centre for Plastic Electronics, Imperial College London, London SW7 2AZ, United Kingdom, [‡]National Physical Laboratory (NPL), Teddington, Middlesex TW11 0LW, United Kingdom, [§]Department of Materials and Centre for Plastic Electronics, Imperial College London, London Royal School of Mines, London SW7 2AZ, United Kingdom, [⊥]Department of Chemistry and Centre for Plastic Electronics, Imperial College London, London SW7 2AZ, United Kingdom, and [#]Department of Materials Science and Engineering, KAIST, Daejeon 305-701, Republic of Korea

ABSTRACT We study the molecular order and morphology in poly(3-hexylthiophene) (P3HT) and poly(3-hexylselenophene) (P3HS) thin films and their blends with [6,6]-phenyl-C_{61}-butyric acid methyl ester (PCBM). We find that substitution of the sulfur atoms in the thiophene rings of P3HT by heavy selenium atoms increases the tendency of the molecules to form better ordered phase; interestingly, their overall fraction of ordered phase is much lower than that of P3HT-based films. The higher tendency of P3HS molecules to order (aggregate) is consistent with more planar chain conformation simulated. The lower fraction of ordered phase (or the higher fraction of disordered phase) in P3HS-based films is clearly identified by in-plane skeleton Raman modes under resonant excitation conditions, such as a smaller ratio of the C═C modes associated with the ordered (~1422 cm^{-1}) and disordered (~1446 cm^{-1}) phases ($I_{1422cm^{-1}}/I_{1446cm^{-1}}$ = 1.4 for P3HS and 0.6 for P3HS:PCBM), compared with P3HT-based films ($I_{1449cm^{-1}}/I_{1470cm^{-1}}$ = 2.5 for P3HT and 1.0 for P3HT:PCBM) and a larger Raman dispersion of the C═C mode: P3HS (17 cm^{-1}) *versus* P3HT (6 cm^{-1}) and P3HS:PCBM (36 cm^{-1}) *versus* P3HT:PCBM films (23 cm^{-1}). The higher fraction of disordered phase in P3HS prevents the formation of micrometer-sized PCBM aggregates in blend films during thermal annealing. Importantly, this lower fraction but better quality of ordered phase in P3HS molecules strongly influences P3HS:PCBM photovoltaic performance, producing smaller short-circuit current (J_{sc}) in pristine devices, but significantly larger increase in J_{sc} after annealing compared to P3HT:PCBM devices. Our results clarify the effects of heavy atom substitution in low band gap polymers and their impact on blend morphology and device performance. Furthermore, our study clearly demonstrates resonant Raman spectroscopy as a simple, but powerful, structural probe which provides important information about "fraction/quantity of ordered phase" of molecules, not easily accessible using traditional X-ray-based techniques.

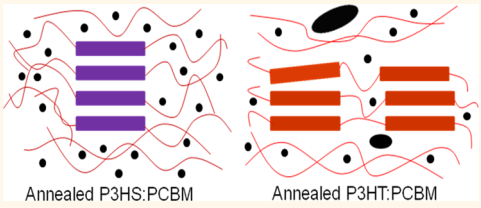

KEYWORDS: poly(3-hexylselenophene) · poly(3-hexylthiophene) · [6,6]-phenyl-C_{61}-butyric acid methyl ester · molecular order · resonant Raman spectroscopy

Conjugated polymer:fullerene blend films are promising systems for novel and low-cost organic solar cells.[1,2] While the efficiency of organic solar cells is still relatively low (~8%),[3] conjugated polymers offer the advantage that they can be readily modified through chemical design or film processing conditions, thus providing opportunities for further improvement.[1,2] It is, however, crucial to gain a thorough understanding of the effect of molecular conformations (*e.g.*, through atomic substitution or verifying processing conditions) on their properties and device performance. Such knowledge will advance our understanding of this interesting class of materials and provides important guidelines for future processing optimization and for synthesizing entirely new photovoltaic compounds.

Photovoltaic cells comprising poly(3-hexylthiophene) (P3HT):[6,6]-phenyl-C_{61}-butyric acid methyl ester (PCBM) blends display relatively high efficiencies[4,5] and are thus one of the most studied polymer:fullerene binary systems. For this reason, they provide a good model system for the detailed study of relevant structure properties−performance relationships. For example, it has been shown that the regioregularity of the side chain substitution of P3HT has a significant

* Address correspondence to ji-seon.kim@imperial.ac.uk.

Received for review July 9, 2012 and accepted October 24, 2012.

Published online October 24, 2012
10.1021/nn304024g

© 2012 American Chemical Society

effect on its molecular order, microstructure, electronic structure, and device efficiency in P3HT:PCBM films.[5−8] It is also well-known that thermal annealing and solvent annealing of P3HT:PCBM films can significantly increase the degree of molecular order of P3HT and lead to significant improvement in device efficiency.[4−7,9,10]

More recently, Heeney *et al.* has synthesized poly(3-hexylselenophene) (P3HS), where sulfur atoms in the thiophene units of P3HT are substituted with selenium atoms.[11] They found that P3HS absorbs at longer wavelengths than P3HT, indicating a band gap of 1.6 eV (compared to 1.9 eV for P3HT) while leaving the highest occupied molecular orbital (HOMO) energy essentially unchanged. The latter is important, as it has been suggested that the magnitude of the gap between the HOMO energy of electron-donating materials (here, P3HT and P3HS) and the lowest unoccupied molecular orbital (LUMO) of electron-accepting materials (here, fullerene) is proportional to the magnitude of the open-circuit voltage (V_{OC}) of polymer:fullerene solar cells.[12] Therefore, P3HS absorbs at longer wavelengths (for better photon harvest) than P3HT without sacrificing the V_{OC} of the polymer:fullerene solar cells. In addition, P3HS has been reported to display a better photostability than P3HT.[11] Importantly, Ballantyne *et al.* demonstrated that active layers of a relatively high molecular weight P3HS and PCBM have a similar V_{OC} and a larger short-circuit current density (J_{SC}) than corresponding P3HT:PCBM blends, albeit at the expense of a smaller fill factor (FF). As a consequence, similar power conversion efficiencies (PCE) of the solar cells are obtained for both systems.[13]

Here, we aim to understand the fundamental effect of the substitution of selenium atoms on the thin film morphology. We study these issues by performing optical absorption, wide-angle X-ray scattering (WAXS), (resonant) Raman and optical microscopy measurements, and combining these with density functional theory (DFT) calculations. The results obtained are then compared with the performance of the P3HS:PCBM and P3HT:PCBM solar cells. We find that substitution of the sulfur atoms in the thiophene rings of P3HT by selenium atoms increases the tendency of the molecules to aggregate and form better ordered phase; however, their overall ordered fraction is lower than that of films comprising P3HT. This has drastic consequences on the solid-state structural development of such blends. The higher tendency of P3HS molecules to aggregate is consistent with the more planar chain conformation calculated using DFT. We propose morphological models for the P3HT:PCBM and P3HS:PCBM films (both pristine and annealed), which are well correlated to their device performances observed. We also show that resonant Raman spectroscopy is a unique and powerful structural probe for investigating the polymer morphology in thin films.

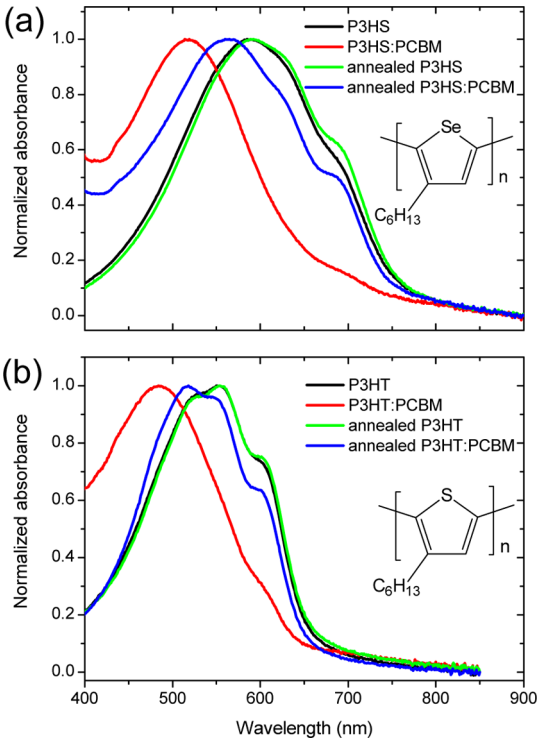

Figure 1. (a) Optical absorption spectra of P3HS and P3HS:PCBM thin films (pristine and annealed) and (b) optical absorption spectra of P3HT and P3HT:PCBM thin films (pristine and annealed). Chemical structures of P3HS and P3HT are also shown.

RESULTS AND DISCUSSION

Absorption Spectra of Thin Films. We first compare the absorption spectra of P3HS films to P3HT films (neat films, annealed films, blend films, and annealed blend films). Figure 1a shows the normalized absorption spectra of P3HS and P3HS:PCBM films (pristine and annealed). Pristine neat P3HS films feature an absorption peak at ~585 nm and an absorption shoulder at ~694 nm, which are ~61 and ~87 nm red-shifted compared with those (~524 and ~607 nm) of neat P3HT films (Figure 1b). This result is consistent with P3HS having a band gap (E_g) lower than that of P3HT. The P3HS absorption shoulder at ~694 nm can be attributed to absorption by aggregates (higher molecular order phase), analogous to the origin of the absorption shoulder at ~607 nm in P3HT film.[5−7,14] After thermal annealing, the absorption at ~694 nm relative to the ~585 nm is only slightly increased, which is similar to the change of the absorption spectra when P3HT films are annealed (Figure 1b), indicating that the degree of molecular order is not significantly hindered in as-cast films.

After blending P3HS polymer with PCBM, the absorption peak blue shifts by ~67 to ~518 nm (or the relative absorption at the lower energy region decreases) and the magnitude of the absorption shoulder at ~694 nm relative to that of the absorption peak is significantly reduced (Figure 1a). This suggests

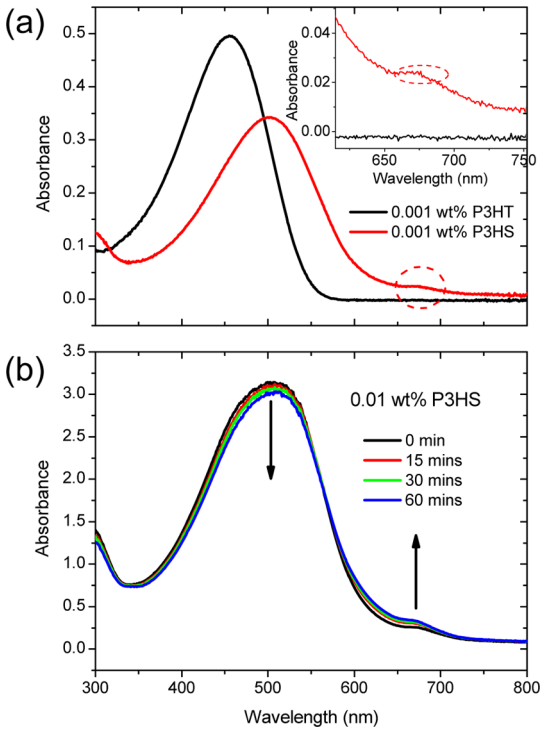

Figure 2. (a) Optical absorption spectra of 0.001 wt % P3HS and 0.001 wt % P3HT in chlorobenzene. Inset shows an enlarged view of the absorption at long wavelength region. (b) Optical absorption spectra of 0.01 wt % P3HS in chlorobenzene as a function of storage time.

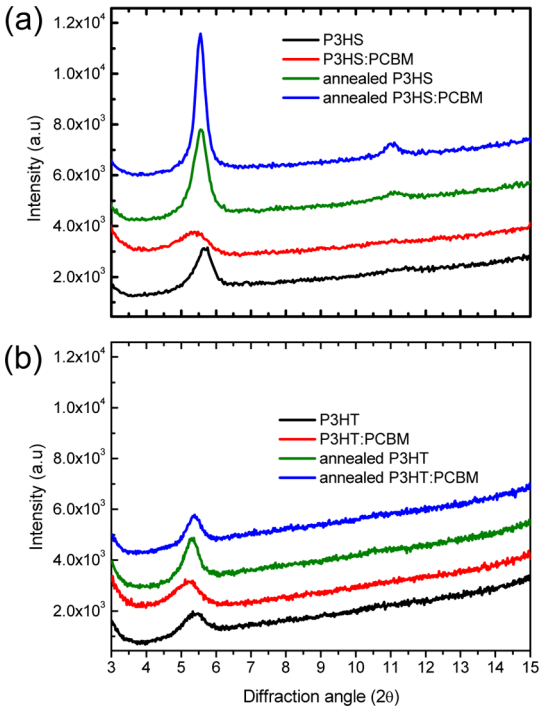

Figure 3. (a) WAXS diffractograms of P3HS and P3HS:PCBM films (both pristine and annealed, data collection time 15 min). (b) WAXS diffractograms of P3HT and P3HT:PCBM films (both pristine and annealed, data collection time 60 min).

that the ordering of P3HS is strongly hindered by the presence of PCBM, which is similar to the behavior of P3HT:PCBM blend films (Figure 1b).[5−7] After annealing P3HS:PCBM films, the absorption peak red shifts to ∼565 nm and the magnitude of the absorption shoulder relative to the absorption peak increases significantly (Figure 1a), implying a strong recovery of molecular order after thermal annealing as also observed for P3HT:PCBM films after annealing (Figure 1b).[5−7]

Absorption Spectra of Solutions. To gain more insight into the aggregation behavior of P3HS and P3HT, we also measured their absorption spectra in dilute solutions. Figure 2a shows the absorption spectra of P3HS and P3HT solutions at 0.001 wt % concentration in chlorobenzene. The absorption peak of 0.001 wt % P3HS solution is at ∼503 nm, which is at much longer wavelength than that of 0.001 wt % P3HT solution (∼456 nm). This suggests that the E_g of P3HS is intrinsically lower than that of P3HT, as the effects due to intermolecular interactions can be largely reduced at such low concentrations. Interestingly, we observed some weak absorption at ∼676 nm even for the 0.001 wt % P3HS solution (Figure 2a and inset), implying that there is still some aggregation present at such a low concentration. On the contrary, there is no evidence of absorption features at longer wavelengths for the P3HT solution at the same concentration (Figure 2a and inset), confirming a high degree of molecular order formed only in the solid state.

Figure 2b shows the absorption spectra of 0.01 wt % P3HS in chlorobenzene as a function of storage time. Similar to the absorption spectrum of the 0.001 wt % P3HS solution, we observed an absorption feature at ∼676 nm. Interestingly, the magnitude of absorption from this feature relative to the main absorption peak at ∼503 nm increases with storage time, suggesting that the formation of aggregates progresses gradually with time (although slow). On the contrary, we did not observe such absorption changes in the 0.01 wt % P3HT solution (data not shown).

To investigate further the aggregation behavior of P3HS and P3HT molecules, we also performed Raman measurements on P3HS and P3HT solutions with concentrations varying from 0.001 to 1 wt % (see Figure S1 and details in Supporting Information). The Raman results of P3HS and P3HT in solutions are consistent with the solution absorption spectra, showing that P3HS has a higher tendency to order (aggregate) in solution than P3HT.

WAXS of Thin Films. We now move to study the crystallization of the thin films in order to understand the effect of the selenium substitution on the molecular order in the solid state. Figure 3a shows the WAXS spectra (peaks arise from lamellar packing) of P3HS and P3HS:PCBM (pristine and annealed). The crystalline quality (quality of lamellar packing)[15] of all of the P3HS and P3HS:PCBM films tends to be better than that of the corresponding P3HT and P3HT:PCBM

films (Figure 3b), as deduced from the stronger scattering signals recorded for P3HS and P3HS:PCBM films at shorter collection times and the sharper peaks compared to those measured for P3HT and P3HT:PCBM films. Note also the presence of higher order reflections in the diffractograms of annealed P3HS systems. It is also important to notice that, although more intensive XRD peaks can indicate better quality (or larger domains) of crystalline phase, they do not necessarily indicate the higher fraction of crystalline phase (or the lower fraction of amorphous phase) formed in the molecules. To gain information about the fraction of crystalline/amorphous phases, we used the resonant Raman spectroscopy. Our resonant Raman data clearly show the strong appearance of higher conformational disorder in the P3HS-based films compared with P3HT-based films (as shown in the next sections), indicating higher fraction of amorphous (disordered) phase present in the P3HS-based films despite its higher XRD peak intensities. The better lamellar packing order in P3HS films and blends appears to be consistent with its strong tendency to aggregate in solution, as shown in previous sections, with the lamellar packing order increasing in the order: P3HS:PCBM < P3HS < annealed P3HS ≤ annealed P3HS:PCBM. We also observed similar trend of lamellar packing order in the films composed of P3HT (Figure 3b).

Note that annealing tends to enhance the lamellar packing order of films comprising P3HS more significantly than that of P3HT (compare Figure 3a,b). It is consistent with the observation reported by Lilliu *et al.* showing, by using grazing incidence X-ray diffraction (GI-XRD), that the crystalline domain sizes and crystallization dynamics of P3HS and P3HT are broadly similar even when using different film preparation protocols.[15] The authors also find that the domain sizes increase significantly with thermal annealing.[15,16]

Raman Spectra of Thin Films. To further understand the effect of the selenium substitution on the degree of molecular order, we measured the Raman spectra of the films under nonresonant and resonant excitation conditions. Figure 4a shows the normalized Raman spectra of P3HS and P3HT thin films excited at 633 nm. In general, the Raman spectrum of P3HS is very similar to that of P3HT due to their similar chemical structures. However, there are two main differences: (i) the positions of the two main in-plane ring skeleton modes of P3HS are shifted to lower wavenumbers by ~25 and ~19 cm^{-1}, respectively, appearing at ~1420 cm^{-1} (symmetric C═C stretch mode) and at ~1362 cm^{-1} (C−C intraring stretch mode) with respect to the C═C (~1445 cm^{-1}) and C−C (~1381 cm^{-1}) modes of P3HT; (ii) there is no ~728 cm^{-1} mode (C−S−C deformation) for P3HS due to the absence of sulfur atoms.[17,18] Herein we focus on these two main in-plane ring skeleton modes, as they have been shown to be sensitive to the π-electron delocalization (effective conjugation length) of the molecules.[6,19,20]

Figure 4b shows the normalized Raman spectra of P3HS and P3HS:PCBM films (pristine and annealed) under 633 nm excitation. All of the Raman spectra of the C═C and the C−C modes are very similar and have the same peak positions. The full width at half-maximum (fwhm) of the C═C mode increases very slightly when P3HS (30 cm^{-1}) is blended with PCBM (31 cm^{-1}) and decreases slightly after annealing the P3HS and P3HS:PCBM films (by 3 and 4 cm^{-1}, respectively; both have fwhm of 27 cm^{-1}). These trends in the peak positions and fwhm are also very similar to those observed in P3HT films under the same excitation conditions (Figure 4c). The insensitivity of the Raman spectra to the annealing and blending processes can be understood by the fact that under 633 nm excitation the Raman probes mainly the ordered phase of molecules (which absorbs at longer wavelengths; see Figure 1a,b), so that the Raman signals are less sensitive to the disordered phase in the films. No Raman signals were observed from PCBM film under the same excitation conditions.

Figure 4d shows the normalized Raman spectra of P3HS and P3HS:PCBM films (pristine and annealed) under 488 nm excitation. Note that the 488 nm excitation wavelength closest to the absorption maximum of P3HS in pristine P3HS:PCBM blend films (Figure 1a), that is, in strong resonance with electronic transitions of the most disordered P3HS phase, allows us to selectively excite more disordered phase of P3HS in different samples. This resonant Raman spectroscopy (RRS) has been previously demonstrated as a simple, but powerful, technique to quantify the degree of molecular order in P3HT and P3HT:PCBM films.[6,19] It was found that, under resonant conditions, the disordered phase of P3HT with respect to its ordered phase is identified by (a) a large shift in the C═C mode peak position to higher wavenumber (from 1449 to 1470 cm^{-1}), (b) a larger fwhm of the C═C mode (41 *vs* 32 cm^{-1}), (c) a smaller intensity of the C−C mode relative to the C═C mode ($I_{C-C}/I_{C=C}$ = 0.09 *vs* 0.14), and (d) a very large Raman dispersion (~28 *vs* ~6 cm^{-1}) of the C═C mode.

It is important to distinguish and identify different molecular order (or packing) that can be probed by XRD and resonant Raman spectroscopy techniques. The XRD is a technique which probes a long-range intermolecular order (packing between molecules or polymers chains), while the resonant Raman spectroscopy probes mainly the intramolecular conformational order of a molecule or a polymer chain. Such intramolecular conformational order of the molecule or the polymer chain will also influence the intermolecular packing of molecules or polymer chains in thin films. Furthermore, more importantly, the resonant Raman spectroscopy is sensitive not only to well-ordered

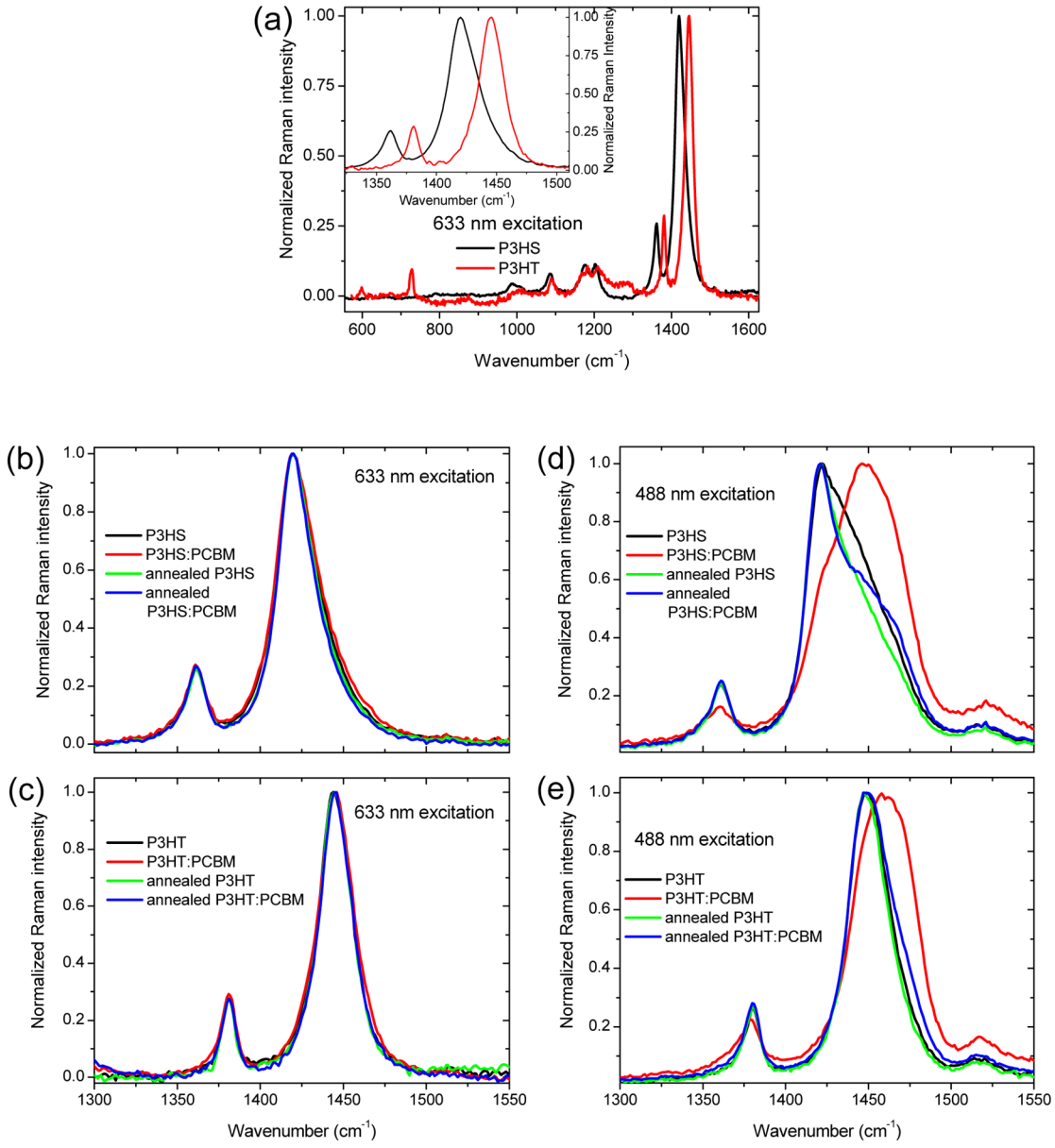

Figure 4. (a) Normalized Raman spectra of P3HS and P3HT thin films under 633 nm excitation. Inset shows an enlarged view of the C═C and the C−C intraring stretch modes. (b,d) Normalized Raman spectra of P3HS and P3HS:PCBM films (pristine and annealed) under 633 and 488 nm excitations, respectively. (c,e) Normalized Raman spectra of P3HT and P3HT:PCBM films (pristine and annealed) under 633 and 488 nm excitations, respectively.

crystalline phase (as similar to the XRD technique) but also to disordered amorphous phase of the molecules. Hence, it provides important information on "fraction/quantity of ordered phase" which is not easily accessible using traditional XRD techniques, as we demonstrated in the next sections.

Here, after blending P3HS with PCBM, we observe similar trends characteristic of the more disordered phase of P3HT; the main peak position of the C═C mode is significantly shifted to higher wavenumber from 1422 cm^{-1} (47 cm^{-1} fwhm, ordered phase) to 1446 cm^{-1} (59 cm^{-1} fwhm, disordered phase) with a largely reduced $I_{1422cm^{-1}}/I_{1446cm^{-1}}$ ratio (from ~1.4 for P3HS to ~0.6 for P3HS:PCBM). The $I_{C-C}/I_{C=C}$ ratio is also reduced from 0.12 to 0.10 (the relative peak intensities are calculated by integrating the peak areas of the C−C and C═C modes). All of these observations are consistent with a higher fraction of disordered P3HS phase present in the P3HS:PCBM blend films. After annealing the P3HS:PCBM blend films, the C═C mode peak position shifts back to lower wavenumber (~1421 cm^{-1}) with an increase in $I_{C-C}/I_{C=C}$ ratio (0.13). A summary of the peak positions and fwhm values of the C═C mode and the $I_{C-C}/I_{C=C}$ ratio of P3HS and P3HS:PCBM films (pristine and annealed) under different excitation wavelengths is shown in Table S1 (Supporting Information).

However, there are noticeable differences between the Raman spectra (the C═C and C−C modes) of films

comprising P3HS compared to those containing P3HT under 488 nm excitation. First, the spectral shape of the C═C mode of neat, pristine P3HS films is highly asymmetric with a long tail at higher wavenumbers (Figure 4d), in contrast to the symmetric spectral shape of the C═C mode of as-cast neat P3HT films (Figure 4e), indicating a higher fraction of disordered phase present in the P3HS films. Second, fwhm of the C═C mode in neat P3HS films is significantly reduced by 7 cm^{-1} (from 47 to 40 cm^{-1}) after annealing, showing that the degree of molecular order is highly enhanced upon the thermal treatment even for the neat polymer film itself. In contrast, there is no considerable change in fwhm of the C═C mode of neat P3HT films after annealing. These results show that thermal annealing can enhance the degree of molecular order in pristine P3HS film more dramatically than in P3HT films. However, the spectral shape of the C═C mode of annealed P3HS film is still asymmetric (due to contributions from the remaining high-energy part), suggesting a considerable portion of disordered phase still present. Third, the C═C mode peak position of P3HS shifts noticeably to high wavenumber (~24 cm^{-1}) after blending with PCBM, which is much larger than that (~9 cm^{-1}) measured when P3HT is blended with PCBM (from 1449 to 1458 cm^{-1}). Such larger shift of this C═C mode peak in P3HS after blending is consistent with the P3HS:PCBM films containing a higher fraction of disordered phase than that of P3HT:PCBM films. It also indicates more pronounced changes in molecular order of P3HS in blend films. Fourthly, after annealing the P3HS:PCBM films, the spectral shape of the C═C mode clearly consists of two components (Figure 4d) with a distinctive high-energy shoulder, different from the annealed P3HT:PCBM films (Figure 4e). These results indicate that there is still a significant amount of disordered P3HS phase present in annealed P3HS:PCBM blend films.

Furthermore, we monitored the Raman dispersion (the degree of the Raman mode shift as a function of excitation wavelength) of the C═C modes. Raman dispersion has been demonstrated as a useful way to probe the degree of molecular order, with larger Raman dispersion implying the presence of a higher fraction of disordered P3HT phase in P3HT:PCBM films.[6] As shown in Figure 5a,b, neat pristine P3HS films feature much larger Raman dispersion than P3HT films. The Raman dispersion of neat P3HS film was reduced significantly when the films were annealed, indicating a reduction of the disordered fractions during the thermal treatment, consistent with the WAXS data (Figure 3a). In contrast, the relatively small Raman dispersion of P3HT films remained mostly unchanged after thermal annealing, suggesting a higher fraction of ordered phase already formed during casting.

The Raman dispersions of both P3HS and P3HT after blending with PCBM is dramatically increased, indicating

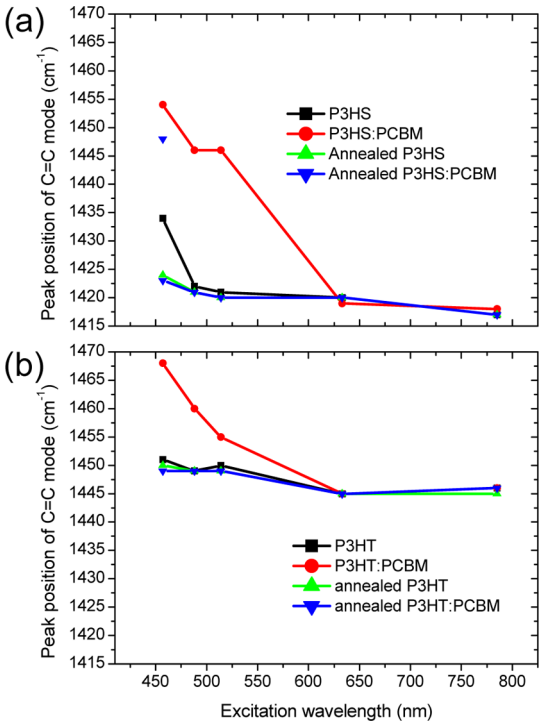

Figure 5. Raman dispersion curves of (a) P3HS and P3HS:PCBM films (pristine and annealed) and (b) P3HT and P3HT:PCBM films (pristine and annealed). Two peak positions of C═C mode under 457 nm excitation are indicated for annealed P3HS:PCBM blend films in (a).

that PCBM has a vitrifying effect on these two polymers (*i.e.*, hinders their ordering). We note that the Raman dispersion of P3HS:PCBM film is 36 cm^{-1}, which is considerably larger than that of P3HT:PCBM film (23 cm^{-1}), again confirming P3HS:PCBM film being more disordered than P3HT:PCBM film. After thermal annealing, the Raman dispersions of both P3HS:PCBM and P3HT:PCBM blend films are reduced and become similar to that of annealed P3HS and annealed P3HT films, respectively, indicating a dramatic recovery in the degree of molecular order. However, the annealed P3HS:PCBM film is still more disordered than annealed P3HT:PCBM film, witnessed by more significant changes in its Raman spectra as a function of excitation wavelength (Figure 6). In general, as the excitation wavelength gets shorter (higher energy), the intensity of the higher energy component of the C═C mode of both annealed P3HS:PCBM and P3HT:PCBM films increases. It is due to the fact that the disordered component (absorbing at higher energies) becomes more resonant with the excitation wavelength. For the annealed P3HS:PCBM film, there is also a small monotonic peak shift of the low energy component of the C═C mode to higher wavenumber with increased excitation energy (from 1419 cm^{-1} for 785 nm to 1423 cm^{-1} for 457 nm). These peak shifts are well-correlated with the increase in intensity of the high-energy component of the C═C mode, resulting from enhanced contribution from the disordered phase. Interestingly, the increase in the

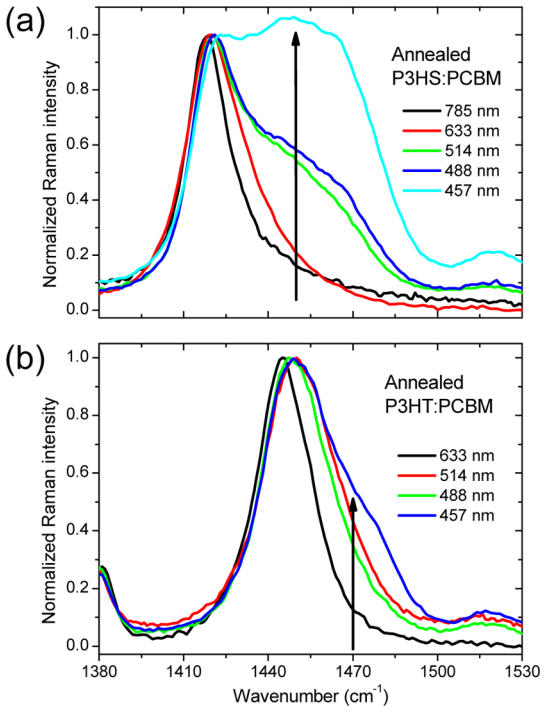

Figure 6. Raman spectra of the C═C mode of (a) annealed P3HS:PCBM blend and (b) annealed P3HT:PCBM films, under different excitation wavelengths.

Raman signal intensity due to the disordered phase is significantly stronger for the annealed P3HS:PCBM film than the annealed P3HT:PCBM film, confirming a higher fraction of disordered P3HS phase still existing in the annealed P3HS:PCBM film. It is important to note that the relative Raman cross section (σ_{rel}) of the ordered and disordered phases in P3HS *versus* that of P3HT needs to be considered to fully quantify the different degree of molecular order in these two polymers.[6]

In summary, the Raman results (RRS, Raman dispersion, and Raman spectra as a function of excitation wavelength) all suggest that P3HS and P3HS:PCBM films (pristine and annealed) comprise lower fractions of ordered phase than the corresponding P3HT and P3HT:PCBM films. WAXS provides complementary information on these fractions with respect to their crystalline quality, which indicates that the crystalline domains of P3HS have better lamellar packing order. It is also important to note that while there are no significant changes in the low-energy absorption after P3HS or P3HT was annealed (Figure 1a,b), there are obvious differences in their XRD diffractograms and resonant Raman spectra. These results indicate that the traditional way of using the low-energy absorption features to estimate degree of molecular order needs to be re-examined.[21]

Optical Micrographs of Annealed Blend Films. Figure 7 shows the optical micrographs of the annealed P3HS:PCBM and P3HT:PCBM films. Annealed P3HS:PCBM films were found to be entirely featureless in contrast to the significant amount of PCBM aggregation

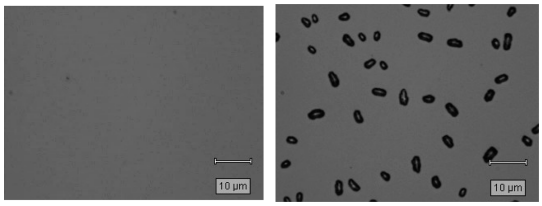

Figure 7. Optical images of the thermal annealed P3HS:PCBM (left) and P3HT:PCBM (right) films.

observed in annealed P3HT:PCBM films. This observation is consistent with the RRS data, suggesting the presence of a higher fraction of disordered polymer phase in annealed P3HS:PCBM films. Indeed, the miscibility of PCBM has been reported to be higher in the disordered regions of polymers,[7,18,22,23] which tend to suppress fullerene aggregation.

DFT Simulations. To understand the effect of the sulfur-to-selenium substitution on the molecular structure and electronic properties, a series of density functional theory (DFT) calculations using oligomers from 3 to 7 units length were performed (full details on the calculation methods and results are described in the Supporting Information). In all of the calculations, the long hexyl side chains were replaced by methyl groups to reduce computation time. From the analysis of inter-ring dihedral angles and inter-ring C−C bond lengths of the optimized structures (Figure S4 and Table S3), we find that the selenium molecules are more planar than their thiophene counterparts. For example, the smaller inter-ring dihedral angles of ∼13−33° in selenophene hepatmer (7Se) were found compared to ∼25−36° in thiophene heptamer (7T). A reduction in the inter-ring C−C bond lengths from ∼1.448 to 1.454 Å between thiophene units to ∼1.439−1.448 Å between selenophene units was also observed. The more planar chain conformation of P3HS oligomers is consistent with the higher tendency of P3HS molecules to form higher ordered phases than the P3HT molecules, as shown in the solution absorption spectra, solution Raman spectra, and WAXS data. As well as the structural changes, the calculations indicate a reduction in the HOMO−LUMO band gap upon selenium substitution (from ∼3.0 to ∼2.5 eV in 7T and 7Se, respectively), which is qualitatively consistent with the trend observed in the optical absorption (Figure 2a). Furthermore, by performing vibrational frequency calculations on the optimized structures, the effects of selenium atom substitution on the Raman spectra were simulated. A shift to lower wavenumbers of the main C═C and C−C vibrational modes was observed in the selenophene molecules (Figure S6a), again consistent with our experimental results (Figure 4a). Finally, the effect of molecular order on Raman peak positions was investigated by monitoring the changes in vibrational frequencies while increasing the chain length or modifying the backbone

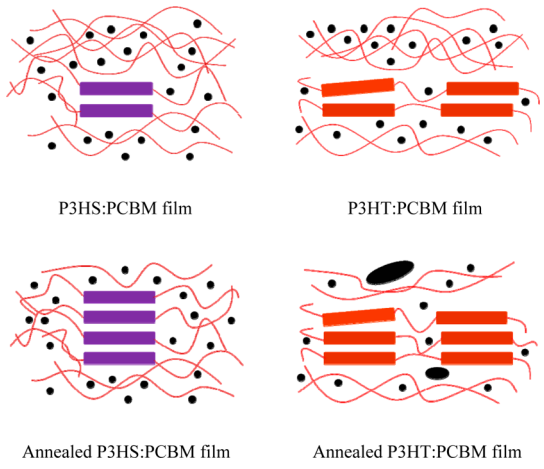

Figure 8. Schematic morphological models (simplified) of P3HS:PCBM and P3HT:PCBM films (pristine and annealed). The rectangular blocks represent the polymer backbones involved in lamellar packing. Curved lines represent disordered polymer chains, and dots/ellipsoids represent PCBM molecules/aggregates. This figure illustrates that P3HS:PCBM films have better lamellar packing order but less quantity of this higher molecular order phase than the corresponding P3HT:PCBM films.

planarity (Figure S6b–e). Previous studies on P3HT have shown that a peak shift of the C=C Raman mode to lower energies, as well as the increase in the $I_{C-C}/I_{C=C}$ ratio, can be used as an indicator for increased molecular order.[6,19] The calculation results indicate that these relationships are preserved in selenophene oligomers, reinforcing the qualitative relationship between C=C Raman peak shift to lower wavenumber (or the increase in $I_{C-C}/I_{C=C}$ ratio) and an increase in molecular order.

Morphological Models and Device Performance. On the basis of experimental measurements (absorption, WAXS, Raman and optical micrographs) and the cross-check with DFT calculations, we propose simplified morphological models for the blend films (pristine and annealed), as shown in Figure 8. Here, our main focus is on the difference in the quality of the lamellar packing order, the fraction/quantity of disordered phase, and the intermixing with PCBM in the blend films. For a thorough morphological model, advanced XRD techniques as well as information on the vertical distribution of the phases are required. It is also worth noting that recent results of Klein suggest that the P3HS domains in annealed P3HS:PCBM bulk films are in the form of nanowhiskers,[24] similar to that of P3HT domains in annealed P3HT:PCBM films.[25]

As shown in Figure 8, the pristine and annealed P3HS:PCBM films comprise a crystalline phase of better lamellar packing order but contain a larger fraction of disordered phase than the pristine and annealed P3HT:PCBM films. It is not clearly understood at the moment why the molecular conformational order is not directly reflected in long-range intermolecular order in P3HS-based films, that is, producing lower molecular conformational order (Raman) but still showing higher long-range order (XRD). We notice that a similar observation has been previously reported in the P3HT system; for example, P3HT can have higher long-range order (XRD) but lower molecular conformational order (or *vice versa*) in P3HT/multiwalled carbon nanotube composites.[26] Here, the molecular conformational order of P3HT was measured by Fourier transform infrared spectroscopy (FTIR). Since the disordered portion of the polymers can intermix relatively well with PCBM, formation of large PCBM crystals is prevented in annealed blends with P3HS. This is consistent with studies by Ballantyne *et al.*, in which they showed that the polymer-rich domains in P3HS:PCBM blend films are less polymer-pure than those in P3HT:PCBM blend films.[18]

The V_{OC} values of P3HS:PCBM and annealed P3HS:PCBM solar cells are slightly smaller than those of the P3HT:PCBM and annealed P3HT:PCBM solar cells (0.61 *vs* 0.68 V for non-annealed devices and 0.54 *vs* 0.60 V for annealed devices) (see Figure S3 and Table S2 in Supporting Information). It has been suggested that the dominant charge carrier loss pathway limiting the V_{OC} of P3HS:PCBM devices is nongeminate recombination.[27,28] The smaller V_{OC} of P3HS:PCBM devices may then be attributed to the more intimate mixing between P3HS and PCBM, which may reduce the probability of charges being extracted and thus increase nongeminate recombination.

The short-circuit current densities of pristine and annealed P3HS:PCBM solar cells are both considerably smaller than those of pristine and annealed P3HT:PCBM solar cells (2.1 *vs* 4.8 mA/cm^2 for non-annealed devices and 6.7 *vs* 8.7 mA/cm^2 for annealed devices). These results are consistent with the higher disordered fraction (although better lamellar packing order) in the P3HS:PCBM films than the P3HT:PCBM films, which may significantly reduce the efficiency of charge transport. Besides, PCBM molecules mix better with the higher fraction of disordered phase in P3HS, which may inhibit electron extraction to the cathode (inducing electron traps). It is worth noting that such trap states need to be taken into account to correctly describe the charge carrier decay dynamics and the current–voltage response in P3HS:PCBM and P3HT:PCBM devices.[27,29,30] There is a more significant increase in short-circuit current density in the P3HS:PCBM device (3.2 times) after thermal annealing than that of the P3HT:PCBM device (1.8 times), consistent with the more significant increase in lamellar packing order of P3HS (which enhances absorption and charge carrier mobility[13]) compared with that of P3HT in P3HT:PCBM films after thermal annealing (Figure 3a,b). However, short-circuit current density of the annealed P3HS:PCBM devices is still lower than that of the annealed P3HT:PCBM devices, agreeing with the higher disordered fraction still existing in an annealed

P3HS:PCBM device and/or the non-optimized phase separation. The non-optimized phase separation (too inmate mixing) is consistent with the faster bimolecular recombination in P3HS:PCBM than in P3HT:PCBM blend devices.[18]

There is no change in the fill factor of P3HS:PCBM devices after thermal annealing, in contrast to the significant increase in the fill factor of P3HT:PCBM devices after thermal annealing, consistent with the similar morphologies before and after annealing the P3HS:PCBM films (large-scale PCBM aggregation is suppressed). However, the still intimate mixing of P3HS molecules with PCBM molecules after annealing the blend film may suppress optimized pathways for charge collection, consistent with its lower fill factor than the annealed P3HT:PCBM device.[31] Interestingly, our proposed morphological models of the films (although simplified) are sufficient to explain the difference in the device parameters of the P3HS:PCBM and P3HT:PCBM devices.

CONCLUSIONS

We show that substituting the sulfur atoms at the thiophene rings of poly(3-hexylthiophene) (P3HT) by selenium atoms (P3HS) enhances the tendency of the molecules to aggregate and to form better quality crystals (better lamellar packing order). However, the overall ordered fraction of films comprising P3HS is lower than that of films comprising P3HT. The higher fraction of disordered phase in P3HS:PCBM films favors the mixing of PCBM molecules with P3HS during thermal annealing, suppressing the formation of micrometer-sized PCBM aggregates, differently from annealed P3HT:PCBM films. We develop simple morphological models for the blend films which agree well with the device performance of P3HS:PCBM and P3HT:PCBM solar cells (both pristine and annealed). The higher tendency of P3HS molecules to aggregate and form better ordered phase is consistent with the more planar chain conformation calculated using DFT. Furthermore, our study clearly demonstrates resonant Raman spectroscopy as a simple, powerful structural probe which is sensitive not only to ordered phase (as similar to X-ray based methods) but also to disordered phase of molecules. Hence, it provides important information on "fraction/quantity of ordered phase" which is not easily accessible using traditional XRD techniques.

METHODS

Film Preparation. P3HS was synthesized by following reported procedures:[11] P3HT was purchased from Merck Chemicals. The weight-average (M_w) and number-average (M_n) molecular weights, polydispersity index (PDI), and regioregularity (RR) were 68.5 kg/mol, 39 kg/mol, 1.76, and 98%, respectively, for the P3HS used here and 54.2 kg/mol, 23.6 kg/mol, 2.29, and 94.2% for the P3HT. PCBM was purchased from API Service, Inc. All of the materials were used as received. For neat films: 12.5 mg of either P3HS or P3HT was dissolved in 1 mL of chlorobenzene. The P3HS and P3HT solutions were heated to 80 and 60 °C overnight (with stirring), respectively, to fully dissolve the materials. The solutions were then spin-coated on quartz substrates at 1500 rpm for 60 s. For the P3HS solution, the solution and the substrate needed to be kept at 80 °C during the spin-coating because of the lower solubility of P3HS in chlorobenzene compared to P3HT. For blend films: 12.5 mg of P3HS (or P3HT) and 12.5 mg of PCBM were mixed in 1 mL of chlorobenzene. For dissolution and deposition, identical procedures as described above for neat systems were followed. Some of the resulting films were then annealed at 140 °C for 30 min inside a nitrogen glovebox. Thicknesses of the films are as follows: neat P3HS ~ 50 nm, neat P3HT ~ 45 nm, P3HS:PCBM ~ 90 nm, and P3HT:PCBM ~ 85 nm. The thicknesses were measured with an Alpha-step 200 profiler (Tencor Instruments).

Solutions. For measurements on solutions, P3HS and P3HT solutions were prepared at 0.001, 0.01, 0.1, and 1 wt % in chlorobenzene. The solutions were heated to 80 and 60 °C overnight (with stirring), respectively, before they were filled into quartz cuvettes (10 mm optical path) for subsequent measurements.

UV–Visible Spectroscopy. Absorption spectra were recorded using a UV–visible spectrophotometer (UV-2550, Shimadzu).

Wide-Angle X-ray Scattering. Measurements were carried out on thin films using a PANALYTICAL X'PERT-PRO MRD diffractometer equipped with a nickel-filtered Cu Kα1 beam and X'CELERATOR detector, using a current I = 40 mA and an accelerating voltage U = 40 kV. Data are expressed as a function of 2θ where θ is half the scattering angle. The exposure times for the area detector measurements were 15 and 60 min for the films comprising P3HS and P3HT, respectively.

Raman Spectroscopy. Raman spectra were recorded at five different excitation wavelengths: 785, 633, 514, 488, and 457 nm (50× objective) with a Renishaw inVia Raman microscope in a backscattering configuration. The excitation conditions were as follows: at 785 nm, 0.93 mW, acquisition time of 1 s, and data accumulated over five acquisitions; at 633 nm, 0.1 mW and acquisition time of 3 s; at 514 and 488 nm, 0.01 mW; at 457 nm, 36 μW. For 514, 488, and 457 nm excitations, the laser beam was defocused to a beam diameter of ~8 μm to avoid photodegradation of the samples, and the data acquisition time was 20 s, with the data accumulated over three acquisitions. The Raman spectra were background-corrected and obtained by averaging the spectra obtained at three different regions in each sample. The spectra at the different regions are very similar, demonstrating the reproducibility of the results. The spectral resolution of the instrument is ~1 cm^{-1}. For Raman measurements on the solutions, 457 nm excitation was used to reduce the strong fluorescence background. The excitation power is 0.18–1.8 mW, and acquisition time is 1–10 s, with the data accumulated over five acquisitions in most cases.

Optical Microscopy. Optical micrographs were obtained using an optical microscope (Leica) with a 50× objective.

Device Fabrication and Characterization. Indium tin oxide (ITO)-coated glass substrates were cleaned with detergent (Mucasol), acetone, and isopropyl alcohol. Poly(3,4-ethylenedioxythiophene)-poly(styrene sulfonate) (PEDOT:PSS, Baytron P TP AI 4083, Bayer AG) was spin-coated on top of the substrates, resulting in layers with a thickness of 30 nm. The films were then annealed at 120 °C for 30 min. The P3HS:PCBM and P3HT:PCBM solutions were spin-coated on top of the PEDOT:PSS films with the same spin-coating conditions as stated above, resulting in layers with a thickness of ~100 nm. Some of the films were thermally annealed at 150 °C for 20 min. Ca (20 nm)/Al (80 nm) electrodes were thermal evaporated onto the films to complete the devices. Performance of the solar cells (encapsulated inside nitrogen chambers) was measured under AM 1.5 conditions at 100 mW/cm^2.

Conflict of Interest: The authors declare no competing financial interest.

Acknowledgment. This work is funded by the EPSRC-NPL Post-Doctoral Research Partnership (EP/G062056/1), the SUPERGEN Excitonic Solar Cell Consortium Grant (EP/G031088/1), and the World Class University (WCU) Program in Korea (Grant No. R32-10051).

Supporting Information Available: (1) Raman spectra of P3HS and P3HT solutions. (2) Peak positions and fwhm of the C═C mode and the $I_{C-C}/I_{C=C}$ values of P3HS and P3HS:PCBM films under different Raman excitation wavelengths. (3) Device characteristics of P3HS:PCBM and P3HT:PCBM solar cells (pristine and annealed) measured under AM 1.5 conditions at 100 mW/cm^2, and (4) full details on the DFT calculation methods and results. This material is available free of charge *via* the Internet at http://pubs.acs.org.

REFERENCES AND NOTES

1. Gunes, S.; Neugebauer, H.; Sariciftci, N. S. Conjugated Polymer-Based Organic Solar Cells. *Chem. Rev.* **2007**, *107*, 1324–1338.
2. Mayer, A. C.; Scully, S. R.; Hardin, B. E.; Rowell, M. W.; McGehee, M. D. Polymer-Based Solar Cells. *Mater. Today* **2007**, *10*, 28–33.
3. He, Z.; Zhong, C.; Huang, X.; Wong, W.-Y.; Wu, H.; Chen, L.; Su, S.; Cao, Y. Simultaneous Enhancement of Open-Circuit Voltage, Short-Circuit Current Density, and Fill Factor in Polymer Solar Cells. *Adv. Mater.* **2011**, *23*, 4636–4643.
4. Ma, W. L.; Yang, C. Y.; Gong, X.; Lee, K.; Heeger, A. J. Thermally Stable, Efficient Polymer Solar Cells with Nanoscale Control of the Interpenetrating Network Morphology. *Adv. Funct. Mater.* **2005**, *15*, 1617–1622.
5. Kim, Y.; Cook, S.; Tuladhar, S. M.; Choulis, S. A.; Nelson, J.; Durrant, J. R.; Bradley, D. D. C.; Giles, M.; McCulloch, I.; Ha, C. S.; *et al.* Strong Regioregularity Effect in Self-Organizing Conjugated Polymer Films and High-Efficiency Polythiophene: Fullerene Solar Cells. *Nat. Mater.* **2006**, *5*, 197–203.
6. Tsoi, W. C.; James, D. T.; Kim, J. S.; Nicholson, P. G.; Murphy, C. E.; Bradley, D. D. C.; Nelson, J.; Kim, J. S. The Nature of In-Plane Skeleton Raman Modes of P3HT and Their Correlation to the Degree of Molecular Order in P3HT:PCBM Blend Thin Films. *J. Am. Chem. Soc.* **2011**, *133*, 9834–9843.
7. Tsoi, W. C.; Spencer, S. J.; Yang, L.; Ballantyne, A. M.; Nicholson, P. G.; Turnbull, A.; Shard, A. G.; Murphy, C. E.; Bradley, D. D. C.; Nelson, J.; *et al.* Effect of Crystallization on the Electronic Energy Levels and Thin Film Morphology of P3HT:PCBM Blends. *Macromolecules* **2011**, *44*, 2944–2952.
8. Chuang, S. Y.; Chen, H. L.; Lee, W. H.; Huang, Y. C.; Su, W. F.; Jen, W. M.; Chen, C. W. Regioregularity Effects in the Chain Orientation and Optical Anisotropy of Composite Polymer/Fullerene Films for High-Efficiency, Large-Area Organic Solar Cells. *J. Mater. Chem.* **2009**, *19*, 5554–5560.
9. Campoy-Quiles, M.; Ferenczi, T.; Agostinelli, T.; Etchegoin, P. G.; Kim, Y.; Anthopoulos, T. D.; Stavrinou, P. N.; Bradley, D. D. C; Nelson, J. Morphology Evolution *via* Self-Organization and Lateral and Vertical Diffusion in Polymer:Fullerene Solar Cell Blends. *Nat. Mater.* **2008**, *7*, 158–164.
10. Li, G.; Yao, Y.; Yang, H.; Shrotriya, V.; Yang, G.; Yang, Y. "Solvent Annealing" Effect in Polymer Solar Cells Based on Poly(3-hexylthiophene) and Methanofullerenes. *Adv. Funct. Mater.* **2007**, *17*, 1636–1644.
11. Heeney, M.; Zhang, W.; Crouch, D. J.; Chabinyc, M. L.; Gordeyev, S.; Hamilton, R.; Higgins, S. J.; McCulloch, I.; Skabara, P. J.; Sparrowe, D.; *et al.* Regioregular Poly(3-hexyl)selenophene: A Low Band Gap Organic Hole Transporting Polymer. *Chem. Commun.* **2007**, 5061–5063.
12. Scharber, M. C.; Muhlbacher, D.; Koppe, M.; Denk, P.; Waldauf, C.; Heeger, A. J.; Brabec, C. J. Design Rules for Donors in Bulk-Heterojunction Solar Cells—Towards 10% Energy-Conversion Efficiency. *Adv. Mater.* **2006**, *18*, 789–794.
13. Ballantyne, A. M.; Chen, L.; Nelson, J.; Bradley, D. D. C.; Astuti, Y.; Maurano, A.; Shuttle, C. G.; Durrant, J. R.; Heeney, M.; Duffy, W.; *et al.* Studies of Highly Regioregular Poly(3-hexylselenophene) for Photovoltaic Applications. *Adv. Mater.* **2007**, *19*, 4544–4547.
14. Clark, J; Silva, C; Friend, R. H.; Spano, F. C. Role of Intermolecular Coupling in the Photophysics of Disordered Organic Semiconductors: Aggregate Emission in Regioregular Polythiophene. *Phys. Rev. Lett.* **2007**, *98*, 206406.
15. Lilliu, S.; Agostinelli, T.; Verploegen, E.; Pires, E.; Hampton, M.; Al-Hashimi, M.; Heeney, M. J.; Toney, M. F.; Nelson, J.; Macdonald, J. E. Effects of Thermal Annealing upon the Nanomorphology of Poly(3-hexylselenophene)-PCBM Blends. *Macromol. Rapid Commun.* **2011**, *32*, 1454–1460.
16. Lilliu, S.; Agostinelli, T.; Pires, E.; Hampton, M.; Nelson, J.; Macdonald, J. E. Dynamics of Crystallization and Disorder during Annealing of P3HT/PCBM Bulk Heterojunctions. *Macromolecules* **2011**, *44*, 2725–2734.
17. Baibarac, M.; Lapkowski, M.; Pron, A.; Lefrant, S.; Baltog, I. SERS Spectra of Poly(3-hexylthiophene) in Oxidized and Unoxidized States. *J. Raman Spectrosc.* **1998**, *29*, 825–832.
18. Ballantyne, A. M.; Ferenczi, T. A. M.; Campoy-Quiles, M.; Clarke, T. M.; Maurano, A.; Wong, K. H.; Zhang, W. M.; Stingelin-Stutzmann, N.; Kim, J. S.; Bradley, D. D. C.; *et al.* Understanding the Influence of Morphology on Poly(3-hexylselenothiophene):PCBM Solar Cells. *Macromolecules* **2010**, *43*, 1169–1174.
19. Gao, Y.; Grey, J. K. Resonance Chemical Imaging of Polythiophene/Fullerene Photovoltaic Thin Films: Mapping Morphology-Dependent Aggregated and Unaggregated C═C Species. *J. Am. Chem. Soc.* **2009**, *131*, 9654–9662.
20. Yacoby, Y.; Ehrenfreund, E. In *Light Scattering in Solids VI*, Cardona, M., Gfintherodt, G., Eds.; Springer: Berlin/Heidelberg, 1991; Vol. 68, p 73.
21. Gaudin, O. P. M.; Samuel, I. D. W.; Amriou, S.; Burn, P. L. Thickness Dependent Absorption Spectra in Conjugated Polymers: Morphology or Interference? *Appl. Phys. Lett.* **2010**, *96*, 053305.
22. Treat, N. D.; Brady, M. A.; Smith, G.; Toney, M. F.; Kramer, E. J.; Hawker, C. J.; Chabinyc, M. L. Interdiffusion of PCBM and P3HT Reveals Miscibility in a Photovoltaically Active Blend. *Adv. Energy Mater.* **2011**, *1*, 82–89.
23. Chen, D.; Nakahara, A.; Wei, D.; Nordlund, D.; Russell, T. P. P3HT/PCBM Bulk Heterojunction Organic Photovoltaics: Correlating Efficiency and Morphology. *Nano Lett.* **2011**, *11*, 561–567.
24. Klein, M. F. G.; Pfaff, M.; Muller, E.; Czolk, J.; Reinhard, M.; Valouch, S.; Lemmer, U.; Colsmann, A.; Gerthsen, D. Poly(3-hexylselenophene) Solar Cells: Correlating the Optoelectronic Device Performance and Nanomorphology Imaged by Low-Energy Scanning Transmission Electron Microscopy. *J. Polym. Sci., Part B: Polym. Phys.* **2012**, *50*, 198–206.
25. Van Bavel, S. S.; Barenklau, M.; de With, G.; Hoppe, H.; Loos, J. P3HT/PCBM Bulk Heterojunction Solar Cells: Impact of Blend Composition and 3D Morphology on Device Performance. *Adv. Funct. Mater.* **2010**, *20*, 1458–1463.
26. Musumeci, A. W.; Silva, G. G.; Liu, J.-W.; Martens, W. N.; Waclawik, E. R. Structure and Conductivity of Multi-Walled Carbon Nanotube/Poly(3-hexylthiophene) Composite Films. *Polymer* **2007**, *48*, 1667–1678.
27. Maurano, A.; Shuttle, C. G.; Hamilton, R.; Ballantyne, A. M.; Nelson, J.; Zhang, W.; Heeney, M.; Durrant, J. R. Transient Optoelectronic Analysis of Charge Carrier Losses in a Selenophene/Fullerene Blend Solar Cell. *J. Phys. Chem. C* **2011**, *115*, 5947–5957.
28. Maurano, A.; Hamilton, R.; Shuttle, C. G.; Ballantyne, A. M.; Nelson, J.; O'Regan, B.; Zhang, W.; McCulloch, I.; Azimi, H.; Morana, M.; Heeney, M.; Durrant, J. R.; *et al.* Recombination Dynamics as a Key Determinant of Open Circuit Voltage in Organic Bulk Heterojunction Solar Cells: A Comparison of Four Different Donor Polymers. *Adv. Mater.* **2010**, *22*, 4987–4992.
29. Shuttle, C. G.; Hamilton, R.; O'Regan, B.; Nelson, J.; Durrant, J. R. Charge-Density-Based Analysis of the Current-Voltage Response of Polythiophene/Fullerene Photovoltaic Devices. *Proc. Natl. Acad. Sci. U.S.A.* **2010**, *107*, 16448–16452.

30. Clarke, T. M.; Jamieson, F. C.; Durrant, J. R. Transient Absorption Studies of Bimolecular Recombination Dynamics in Polythiophene/Fullerene Blend Films. *J. Phys. Chem. C* **2009**, *113*, 20934–20941.
31. Chiu, M.-Y.; Jeng, U.-S.; Su, C.-H.; Liang, K. S.; Wei, K.-H. Simultaneous Use of Small- and Wide-Angle X-ray Techniques To Analyze Nanometerscale Phase Separation in Polymer Heterojunction Solar Cells. *Adv. Mater.* **2008**, *20*, 2573–2578.